A&A 657, A58 (2022)
https://doi.org/10.1051/0004-6361/202141608

Astronomy & Astrophysics

Broad-band analysis of X-ray pulsar 2S 1845–024

Armin Nabizadeh[1], Sergey S. Tsygankov[1,2], Sergey V. Molkov[2], Dmitri I. Karasev[2], Long Ji[3], Alexander A. Lutovinov[2], and Juri Poutanen[1,2,4]

[1] Department of Physics and Astronomy, University of Turku, 20014 Turku, Finland
e-mail: armin.nabizadeh@utu.fi
[2] Space Research Institute of the Russian Academy of Sciences, Profsoyuznaya Str. 84/32, Moscow 117997, Russia
[3] School of Physics and Astronomy, Sun Yat-Sen University, Zhuhai, Guangdong 519082, PR China
[4] Nordita, KTH Royal Institute of Technology and Stockholm University, 10691 Stockholm, Sweden

Received 21 June 2021 / Accepted 12 October 2021

ABSTRACT

We present the results of a detailed investigation of the poorly studied X-ray pulsar 2S 1845−024 based on data obtained at the *NuSTAR* observatory during the type I outburst in 2017. Neither pulse phase-averaged nor phase-resolved spectra of the source show evidence for a cyclotron absorption feature. We also used data obtained from other X-ray observatories (*Swift*, *XMM-Newton* and *Chandra*) to study the spectral properties as a function of orbital phase. The analysis reveals a high hydrogen column density for the source reaching $\sim 10^{24}$ cm^{-2} around periastron. Using high-quality *Chandra* data we were able to obtain an accurate localization of 2S 1845−024 at RA = $18^{\rm h}48^{\rm m}16\overset{\rm s}{.}8$ and Dec = $-2^{\circ}25'25\overset{''}{.}1$ (J2000), which allowed us to use infrared (IR) data to roughly classify the optical counterpart of the source as an OB supergiant at a distance of $\gtrsim$15 kpc.

Key words. accretion, accretion disks – magnetic fields – pulsars: individual: 2S 1845–024 – stars: neutron – X-rays: binaries

1. Introduction

2S 1845−024 (also known as GS 1843−024) is a transient X-ray source discovered with the *Ginga* observatory (Makino & GINGA Team 1988; Koyama et al. 1990a). It belongs to the class of high-mass X-ray binaries (HMXBs). Many of the physical properties of the system and the neutron star (NS) are still unknown. The system contains an X-ray pulsar (XRP) with a spin period $P_{\rm spin} = 94.8$ s (Makino & GINGA Team 1988; Zhang et al. 1996). A series of the Burst and Transient Source Experiment (BATSE) observations performed in 1991−1997 detected ten type I outbursts revealing an orbital period $P_{\rm orbital} = 242.18 \pm 0.01$ d for the system (Finger et al. 1999). More outbursts around periastron passage (orbital phase zero) were detected later by different observatories (e.g., Doroshenko et al. 2008). No type II outbursts have yet been detected from the source. The timing analysis allows the orbital parameters of the system to be determined: the high eccentricity of $e = 0.879 \pm 0.005$ and the projected semi-major axis $a_x \sin i = 689 \pm 38$ lt-s, suggesting a high-mass companion ($M > 7\,M_\odot$) for 2S 1845−024 (Finger et al. 1999; Koyama et al. 1990a).

The companion star in this system has not yet been directly identified. However, the source is classified as a transient Be/XRP based on the outburst pattern and the highly eccentric orbit (Koyama et al. 1990a; Zhang et al. 1996; Finger et al. 1999). In addition, the location of the source in the Corbet (1986) diagram is consistent with a Be/NS binary. The 2−38 keV X-ray spectrum of 2S 1845−024, obtained by the *Ginga* Large Area Counter (LAC), fitted by a power law with a high-energy cutoff model, revealed a large hydrogen column density $N_{\rm H} \simeq (1.5{-}3.0) \times 10^{23}$ cm^{-2} in the direction of the source (Koyama et al. 1990a). Assuming that the lower limit on $N_{\rm H}$ is accounted for by the interstellar medium, Koyama et al. (1990a) estimated the source distance to be about 10 kpc. We emphasize that there is no *Gaia* distance measurements available for this source.

The BATSE observations of 2S 1845−024 also measured a secular long-term spin-up trend at a rate of $\dot{\nu} \sim 2.7 \times 10^{-13}$ Hz s^{-1} during the 1991−1997 period of activity (Finger et al. 1999). Currently, however, the observations provided with the *Fermi* Gamma-ray Burst Monitor (GBM) Accreting Pulsars Program (GAPP[1]; Malacaria et al. 2020) show that the source has been in a spin-down phase during the last six years. It can therefore be inferred that the source underwent a torque reversal before entering to the long-term spin-down trend with a rate of $\dot{\nu} \sim -2.4 \times 10^{-13}$ Hz s^{-1} (Malacaria et al. 2020). Because there are no data available for the source in the period between 51560 and 56154 MJD, Malacaria et al. (2020) estimated that the torque reversal occurred at 53053 ± 250 MJD by extrapolating the spin-up and spin-down log-term trends in the gap between BATSE and GBM observations.

Although there are several X-ray observations available for 2S 1845−024, the properties of the source in the soft and hard X-ray bands have not been fully investigated. Namely, fundamental parameters such as the NS magnetic field strength, the type of the companion star, and the distance to the system have not yet been determined or are still debated. In the study presented here, we used a single *NuSTAR* observation, which was performed during a normal type I outburst on 2017 April 14 as well as several other archival observations obtained with different X-ray satellites to perform a detailed temporal and spectral analysis of 2S 1845−024 in a wide energy band in order to determine its properties.

[1] http://gammaray.nsstc.nasa.gov/gbm/science/pulsars/

2. Observations and data reduction

Since its discovery, 2S 1845−024, has been extensively observed by several instruments such as *NuSTAR*, *XMM-Newton*, *Chandra*, and *Swift*. The summary of the observations used in this work is given in Table 1. Here we focus on the details of the observations obtained by the mentioned X-ray observatories which were performed at different orbital phases (see Fig. 1), calculated using ephemeris $T_{\rm Periastron} = 2449616.98 \pm 0.18$ (JD) (Finger et al. 1999). The temporal and spectral analysis was done using HEASOFT 6.28[2] and XSPEC 12.11.1b[3]. For the spectral analysis, the data were grouped to have at least 25 counts per energy bin in order to use χ^2 statistics unless otherwise stated in the text.

2.1. NuSTAR observations

The *NuSTAR* X-ray observatory consists of two identical and independent co-aligned X-ray telescopes focusing the incident X-rays into two focal plane modules A and B (FPMA and FPMB) (Harrison et al. 2013). The instruments contain four (2 × 2) solid-state cadmium zinc telluride (CdZnTe) pixel detectors operating in a wide energy range of 3−79 keV. *NuSTAR* instruments provide an X-ray imaging resolution of 18″ full width at half maximum (FWHM) and a spectral energy resolution of 400 eV (FWHM) at 10 keV. 2S 1845−024 was observed with *NuSTAR* on 2017 April 14 for a duration of ∼35 ks during the peak of the outburst. In order to reduce the raw data, we followed the standard procedure explained in *NuSTAR* official user guides[4] the *NuSTAR* Data Analysis Software NUSTARDAS v2.0.0 with a CALDB version 20201130. The source and background photons were extracted from circular regions with radii 90″ and 150″, respectively, for both modules.

2.2. Swift observations

2S 1845−024 was observed by the XRT telescope (Burrows et al. 2005) onboard the *Neil Gehrels Swift* Observatory (*Swift*; Gehrels et al. 2004) several times in the period of 2007–2019. In this study, we used five *Swift*/XRT observations, all obtained in the photon counting (PC) mode as listed in Table 1. The corresponding spectra were extracted using the online tools[5] (Evans et al. 2009) provided by the UK Swift Science Data Centre. Because the count rate in all *Swift* observations is below 0.3 count s^{-1}, the data were not affected by the pile-up effect[6]. One of the *Swift*/XRT observations (ObsID 00088089001) was performed simultaneously with the *NuSTAR* observation allowing us to obtain spectral parameters in a wider energy band 0.3−79 keV. The source spectra as observed by *Swift*/XRT and *NuSTAR*/FPMA-B were then fitted simultaneously in the energy ranges 0.3−10 and 4−79 keV, respectively, accounting for differences in normalization.

2.3. XMM-Newton observations

The X-ray Multi-Mirror Mission (*XMM-Newton*) (Jansen et al. 2001) carries three X-ray telescopes each with a medium spectral resolution European Photon Imaging Camera at the focus operating in the range of 0.2−10 keV (EPIC-MOS1, -MOS2 and -pn). 2S 1845−024 was observed by *XMM-Newton* two times in 2006 with the exposure times of ∼23 and ∼16 ks with all three EPIC X-ray instruments. We reduced and analyzed the data following the standard procedure explained in Science Analysis System (SAS) user guide[7] using the software SAS version 17.0.0 and the latest available calibration files. We extracted the source spectra and light curves from a source-centered circular region with a radius of 20″ for all three instruments. The background was likewise extracted from source-free regions of the same radius

Table 1. Observation log of 2S 1845−024.

ObsID	Start date	Start MJD	Exposure (ks)
	NuSTAR		
90201056002	2017-04-14	57857.59	34.71
	XMM-Newton		
0302970601	2006-04-11	53836.75	22.66
0302970801	2006-10-06	54014.39	15.91
	Chandra		
2692	2002-08-18	52504.25	4.96
2689	2002-09-04	52521.42	14.80
2691	2002-09-06	52523.31	14.76
2690	2002-09-12	52529.78	15.09
10512	2009-02-21	54883.40	5.76
	Swift/XRT		
00609139000	2014-08-10	56879.59	0.80
00033739001	2015-04-14	57126.04	0.59
00707545000	2016-08-06	57606.47	1.53
00745966000	2017-04-06	57849.52	0.57
00088089001	2017-04-14	57857.82	1.98
	UKIDSS/UKIRT		
4543927	2006-06-12	53898.468	0.39
6610544	2006-06-12	53898.472	0.36

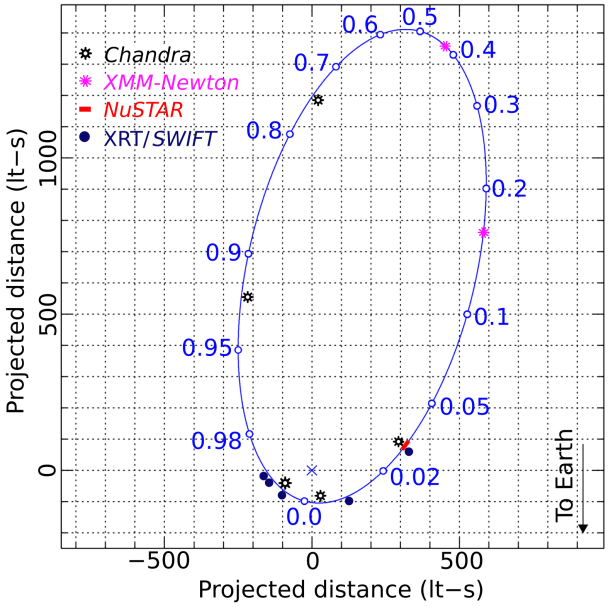

Fig. 1. Orbital phases corresponding to the date of each observation performed by *NuSTAR*, *XMM-Newton*, *Chandra*, and *Swift*/XRT.

[2] https://heasarc.gsfc.nasa.gov/docs/software/heasoft/
[3] https://heasarc.gsfc.nasa.gov/xanadu/xspec/manual/XspecManual.html
[4] https://nustar.ssdc.asi.it/news.php#
[5] https://www.swift.ac.uk/user_objects/
[6] https://www.swift.ac.uk/analysis/xrt/pileup.php
[7] https://xmm-tools.cosmos.esa.int/external/xmm_user_support/documentation/sas_usg/USG/

Table 2. Coordinates and IR magnitudes of the counterpart of 2S 1845−024 based on UKIDSS/GPS and *Spitzer* data.

RA	$18^h48^m16\overset{s}{.}87$
Dec	$-02°25'25\overset{''}{.}2$
l	$30\overset{\circ}{.}4151$
b	$-0\overset{\circ}{.}4031$
H	17.82 ± 0.04
K	15.52 ± 0.03
[3.6] μm	12.74 ± 0.07
[4.5] μm	12.35 ± 0.14
[5.4] μm	11.66 ± 0.11

in the same chips. We note that there are no MOS1 data available for observation ObsID 0302970601.

2.4. Chandra observations

2S 1845−024 was observed by the *Chandra* advanced CCD Imaging Spectrometer (ACIS) several times in 2002 and 2009 (see Table 1) providing a total exposure time of 55.4 ks. In all observations, the source is located in ACIS-S3 except for the observation ObsID 10512 in which the detector ACIS-I3 was used. Following the standard pipeline procedure[8], we reprocessed the data to extract new event files (level 2) using the task CHANDRA_REPRO from the software package CIAO v4.12 with an up-to-date CALDB v4.9.1. We then extracted the source and background spectra from circular regions of 10″ and 30″ in radius, respectively.

2.5. UKIDSS/UKIRT observations

In order to study the type of companion star in 2S 1845−024 using the methods explained in Karasev et al. (2015) and Nabizadeh et al. (2019), the magnitudes of the star in two near-infrared (NIR) filters H and K are required. We took the magnitude of the counterpart in the K filter from the latest public release of the UKIRT Infrared Deep Sky Survey (UKIDSS) catalog UKIDSS/GPS DR11 PLUS[9]. However, the magnitude of the source in the H filter is not present in that catalog. To solve this problem, we performed an additional photometric analysis of UKIDSS image data (id 4543927 observed on 2006 June 12) using PSF-photometry (DAOPHOT II[10]) methods.

Having obtained the instrumental magnitudes of all the stars in the 3′ vicinity of 2S 1845−024, we were able to compare these instrumental magnitudes with those in the standard UKIDSS catalog (HAperMag3). We then selected only the stars brighter than 17 mag in the H-filter for this analysis, excluding overexposed objects. Thus, we estimated a mean correction value and converted the DAOPHOT magnitude (in the H-filter) of the probable counterpart into the real or observed magnitude in the corresponding filter (see Table 2). We emphasize that 2S 1845−024 is not detected in the J filter.

3. Analysis and results

3.1. Pulse profile and pulsed fraction

For the timing analysis, we used *NuSTAR* barycentric-corrected and background-subtracted light curves. The binary motion correction was also applied to the light curves to convert the observed time to the binary-corrected time using the orbital parameters obtained from Finger et al. (1999) and given in Table 3. The long exposure time and high count rate allowed us to determine the spin period of the NS of $P_{\rm spin} = 94.7171(3)$ s. To obtain the spin period and its uncertainty, the standard EFSEARCH procedure from the FTOOL package was applied on 10^3 simulated light curves created by using the count rates and uncertainties of the original 3−79 keV light curve (see e.g., Boldin et al. 2013). Considering the wide energy range of *NuSTAR*, we were able to study the pulse profile of the source as a function of energy. For this, we first extracted the source and background light curves in five energy bands 3−7, 7−18, 18−30, 30−50, and 50−79 keV. We then combined the light curves extracted from the modules FPMA and FPMB in order to increase the statistics.

Table 3. Orbital parameters of 2S 1845−024 (Finger et al. 1999).

Orbital period	242.18 ± 0.01 days
$T_{\rm Periastron}$	2449616.98 ± 0.18 JD
$a_x \sin i$	689 ± 38 lt-s
Longitude of periastron	252.2 ± 9.4 deg
Eccentricity	0.8792 ± 0.0054

The energy-dependent light curves were folded with the obtained pulse period using the task EFOLD from the XRONOS package. Evolution of the pulse profile with energy is shown in the top five panels of Fig. 2. Pulse profiles demonstrate a complicated structure consisting of multiple peaks. The main maximum and minimum are around 0.1−0.2 and 0.6−0.7, respectively, where the zero phase is chosen arbitrarily. As can be seen, the pulse profile depends on energy, with the multi-peak structure becoming more prominent at higher energies. The most significant changes take place around the main minimum and maximum of the profile. This is best illustrated with the hardness ratio constructed using the pulse profiles in 3−7 and 18−30 keV bands as shown in the bottom panel of Fig. 2. The hardness ratio shows two clear hardenings of the emission at the rising part of the main maximum and at the center of the main minimum.

We also calculated the pulsed fraction, determined as $\mathrm{PF} = (F_{\rm max} - F_{\rm min})/(F_{\rm max} + F_{\rm min})$, where $F_{\rm max}$ and $F_{\rm min}$ are the maximum and minimum fluxes of the pulse profile, as a function of energy. In the majority of XRPs, the pulse fraction shows a positive correlation with the energy (Lutovinov & Tsygankov 2009); however, as shown in Fig. 3, the pulsed fraction in 2S 1845−024 has values of around 40%−50% with no prominent dependence on the energy.

3.2. Phase-averaged spectroscopy

The simultaneous observations of 2S 1845−024 obtained with *Swift*/XRT and *NuSTAR* allowed us to perform the spectral analysis in a broad band, 0.3−79 keV, for the first time for the source. The broadband spectrum of 2S 1845−024 shown in Fig. 4 was found to have a shape typical for XRPs (Filippova et al. 2005). According to Koyama et al. (1990a), the source continuum can be fitted by a phenomenological model such as a power law with a high-energy exponential cut-off. However, to find the best-fit model, we tested several continuum models as listed in Table 4. Consequently, the FDCUT model could not fit the spectrum, while CUTOFFPL, NPEX, and COMPTT gave acceptable fits with χ^2 (d.o.f.) of 2098 (1769), 1787 (1766), and 2007 (1768), respectively. The model PO × HIGHECUT fitted the spectrum slightly better with χ^2 (d.o.f.) = 1769 (1767). Therefore, and also to be

[8] https://cxc.cfa.harvard.edu/ciao/threads/index.html
[9] http://surveys.roe.ac.uk/wsa/
[10] http://www.star.bris.ac.uk/~mbt/daophot/

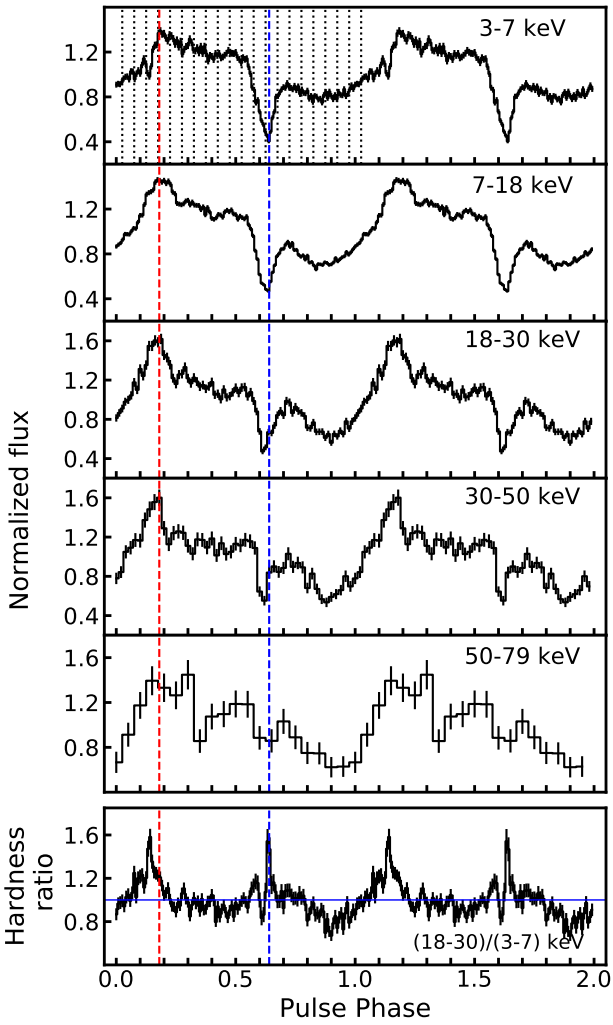

Fig. 2. *Top panels*: pulse profile of 2S 1845−024 in different energy bands obtained from the *NuSTAR* observation. Fluxes are normalized by the mean flux in each energy range. The red and blue dashed lines show the main maximum and minimum in the 3−7 keV band, respectively. The black dotted lines in the uppermost panel show the phase segments used to extract the phase-resolved spectra. *Bottom panel*: hardness ratio of the source over the pulse phase calculated as a ratio of normalized count rates in the pulse profiles in the energy bands 18−30 and 3−7 keV. The hardness ratio of unity is indicated by the horizontal blue solid line.

able to make a comparison between our results and the previous studies, we used this preferred model for both the phase-averaged and the phase-resolved analysis. The Galactic and intrinsic absorption was modeled using photoelectric absorption model TBABS with abundances from Wilms et al. (2000) and atomic cross-sections adopted from Verner et al. (1996). We also used a Gaussian emission component to account for the narrow fluorescent iron line at 6.4 keV.

The best-fit composite model (CONSTANT × TBABS (PO × HIGHECUT + GAUSSIAN)) along the data and the corresponding residuals are shown in Fig. 4 and the best-fit parameters and the corresponding uncertainties at 68.3% (1σ) confidence level are given in Table 5. The fit revealed a large hydrogen column density $N_{\rm H} = (22.7 \pm 0.7) \times 10^{22}\,{\rm cm}^{-2}$. We note that the Galactic mean value in the direction of the source is $1.81 \times 10^{22}\,{\rm cm}^{-2}$ (Willingale et al. 2013) which is significantly lower than what we obtained. This discrepancy could be due to a significant intrinsic absorption in the system. To explore

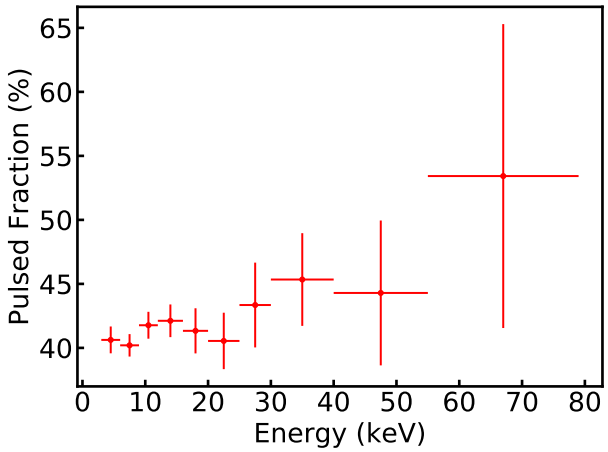

Fig. 3. Energy dependence of the pulse fraction of 2S 1845−024 obtained from the *NuSTAR* observation.

this hypothesis, we studied variations of the column density as a function of orbital phase.

We used the 11 archival observations (see Table 1) performed at different orbital phases as listed in Table 6. As the data cover only the soft X-ray band below 10 keV, we modeled the spectra using a simple composite model TBABS × (PO + GAUSSIAN). We note that the *NuSTAR* spectra were also fitted using the same model in the energy range 4−10 keV. Due to the lack of high count statistics in some observations we were unable to detect the iron emission line and therefore fixed the line centroid energy and width to our best-fit values from the joint *Swift*+*NuSTAR* data. We thus obtained the column density for different orbital phases, and present these in Table 6. The corresponding X-ray flux for each observation was also calculated in the energy range 0.3−10 keV and is reported in the same table. The data show a strong dependence of $N_{\rm H}$ on the orbital phase as well a correlation with the flux (see Table 6). For those observations with lower exposure time, we binned the spectra to have at least 1 count s^{-1} and used W-statistics (Wachter et al. 1979) in order to get more reliable fits.

We emphasize that the best-fit model showed no evidence of a cyclotron resonant scattering feature (CRSF) in the broad-band source spectra (see Fig. 4). However, we continued searching for the possible cyclotron line following the steps explained by Doroshenko et al. (2020). Nevertheless, we did not detect any absorption feature at any energy with significance above $\sim 2.4\sigma$.

3.3. Phase-resolved spectroscopy

Phase-resolved spectroscopy is a useful technique for studying the spatial properties of the emitting region of the NS. Based on the good counting statistics, we extracted 20 equally spaced phase bins (see upper panel in Fig. 2) from the available *NuSTAR* observation of 2S 1845−024. Each spectrum was fitted with our best-fit model (CONSTANT × TBABS (PO × HIGHECUT + GAUSSIAN); see Sect. 3.2). Similar to the phase-average spectral analysis, we fixed the iron line width at 0.1 keV for all 20 spectra. The evolution of the fit parameters are shown in Fig. 5.

The hydrogen column density $N_{\rm H}$ varies in the range of $(15-31) \times 10^{22}\,{\rm cm}^{-2}$ showing a marginally significant deviation from a constant. The photon index Γ shows a similar behavior to that of $N_{\rm H}$, varying from ~0.7 at the main maximum to ~1.5 at the second minimum of the pulse. The cutoff energy $E_{\rm cut}$ remains

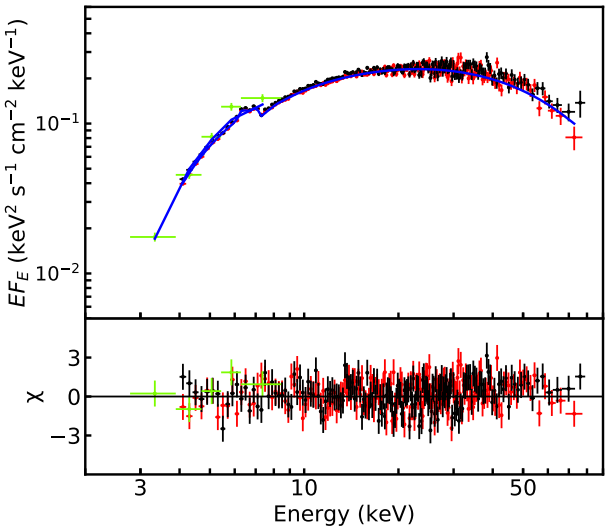

Fig. 4. *Top panel*: broad band X-ray spectrum of 2S 1845−024 extracted from *Swift*/XRT (green crosses) and *NuSTAR*/FPMA and FPMB (red and black crosses). The solid blue line represents the best-fit model CONSTANT × TBABS × (PO × HIGHECUT + GAU). *Bottom panel*: residuals from the best-fit model in units of standard deviations. We emphasize that the *Swift*/XRT spectrum is obtained in the range 0.3−10 keV; however, there are not enough soft X-ray photons below 3 keV because the spectrum is highly absorbed.

Table 4. Phenomenological models used to fit the source spectral continuum.

Model	Photon energy distribution
CUTOFFPL	$N(E) = KE^{-\alpha}\exp(-E/\beta)$
PO × HIGHECUT	$M(E) = KE^{-\alpha}\exp[(E_c - E)/E_f]$, $(E \geq E_c)$
	$M(E) = KE^{-\alpha}$, $(E \leq E_c)$
NPEX	$N(E) = (A_1E^{-\alpha_1} + A_2E^{+\alpha_2})\exp(-E/kT)$
FDCUT	$N(E) = A_{PL}E^{-\Gamma}/[\exp((E - E_{cut})/E_{fold}) + 1]$
COMPTT	Comptonization model from Titarchuk (1994)

almost constant around 8 keV throughout the pulse with variations between 5.8 and 9.5 keV. The folding energy E_{fold} is more variable reaching ∼48 keV near the second minimum of the pulse and decreasing down to 19 keV at the main maximum.

Because there is a possible strong internal correlation between N_H and Γ in the soft X-ray band, we constructed the confidence contour plot of these two parameters using the spectra of the phases 0.5 and 0.8 where these parameters have different values (see Fig. 6). We see that although the values of N_H for two phases agree within 2σ confidence level, the photon index is significantly different, pointing to the intrinsic variability of the spectrum.

3.4. X-ray position and IR companion

Due to the poor localization of 2S 1845−024, the nature of the optical counterpart in this system remains unclear. 2S 1845−024 is located in the Scutum region which is crowded by transient XRPs and their companions (Koyama et al. 1990b). In order to determine the source position from the X-ray data, we selected one of the *Chandra* observations (ObsID 2689). Using the task CELLDETECT standard routines[11], we obtained the source position at RA = 18^{h}48^{m}16^s.8 and Dec = −2°25′25″.1 (J2000). A total uncertainty of 1″ (at 90% confidence level radius), including the systematic uncertainty of *Chandra* absolute positions[12], was obtained for the localization accuracy of the source.

We also obtained the astrometrically corrected source coordinates from the averaged image of all available *Swift*/XRT observations using the online XRT products generator[13]. Based on this, the source is located at RA = 18^{h}48^{m}16^s.91 and Dec = −2°25′26″.1 (J2000) with an error radius of 2″.5 at 90% confidence level, which is fully consistent with the *Chandra* results (see Fig. 7).

Table 5. Best-fit parameters for the joint *Swift*/XRT and *NuSTAR* phase-averaged spectrum approximated with the CONSTANT × TBABS (POWERLAW × HIGHECUT + GAUSSIAN) model.

Model	Parameters	Unit	Value
CONSTANT	*NuSTAR* [(a)]		1.015 ± 0.003
	Swift/XRT [(b)]		0.69 ± 0.03
TBABS	N_H	10^{22} cm^{-2}	22.7 ± 0.7
POWERLAW	Γ		1.23 ± 0.02
	Norm	(×10^{-2})	3.6 ± 0.2
HIGHECUT	E_{cut}	keV	8.2 ± 0.2
	E_{fold}	keV	28.6 ± 0.8
GAUSSIAN	E_{Fe}	keV	6.35 ± 0.03
	σ_{Fe}	keV	$0.10^{+0.07}_{-0.09}$
	Norm	10^{-4} ph s^{-1} cm^{-2}	1.3 ± 0.3
$F_{0.3-79}$ [(c)]		10^{-9} erg s^{-1} cm^{-2}	1.07 ± 0.01
$F_{0.3-10}$ [(c)]		10^{-10} erg s^{-1} cm^{-2}	4.10 ± 0.09
χ^2			1769
d.o.f.			1767

Notes. [(a)]Cross-calibration normalization constant between *NuSTAR*/FPMA and FMPB. [(b)]Cross-calibration normalization constant between *NuSTAR*/FPMA and *Swift*/XRT. [(c)]Unabsorbed X-ray flux.

3.5. Nature of the IR companion

Using the results of *Chandra* localization and data of the UKIDSS NIR sky survey, we were able to identify the IR counterpart of 2S 1845−024 (see Fig. 7, left panel). The coordinates and magnitudes of the IR counterpart are given in Table 2. The expected class of the star as well as its distance can be estimated using a method that has been successfully applied in a number of sources (see, e.g., Karasev et al. 2015; Nabizadeh et al. 2019).

Comparing the measured color of the source, $(H - K) = 2.30 \pm 0.05$, with the intrinsic colors $(H-K)_0$ of different classes of stars (Wegner 2014, 2015, all values were converted into the UKIRT filter system via relations from Carpenter 2001), we can estimate the corresponding extinction corrections $E(H - K) = (H - K) - (H - K)_0$. 2S 1845−024 is located far from the Galactic bulge, and therefore we can use a standard extinction law (Cardelli et al. 1989) to transform each $E(H-K)$ into the extinction A_K. In turn, comparing absolute magnitudes of the same classes of stars M_K (Wegner 2000, 2006, 2007) with the measured magnitude of the source in the K-filter, we are able to estimate a probable distance D to each class of stars by solving $5-5\log_{10} D = M_K - K + A_K$. The results of this approach are indicated in Fig. 8.

[11] https://cxc.cfa.harvard.edu/ciao/threads/celldetect/

[12] https://cxc.harvard.edu/cal/ASPECT/celmon/

[13] https://www.swift.ac.uk/user_objects/

Table 6. Spectral parameters of 2S 1845−024 as a function of orbital phase.

Observatory	ObsID	Orbital phase	Γ	N_H ($\times 10^{22}$ cm^{-2})	Flux [a] (erg s^{-1} cm^{-2})
Chandra	2691	0.003	0.08 ± 0.39	52 ± 11	$2.4^{+0.6}_{-0.4} \times 10^{-11}$
Swift	00033739001	0.009	$0.7^{+1.0}_{-0.6}$	68^{+22}_{-10}	$2.5^{+3.5}_{-0.9} \times 10^{-10}$
NuSTAR+Swift [b]	90201056002+00088089001	0.029	1.15 ± 0.03	21.0 ± 0.9	$3.14^{+0.06}_{-0.08} \times 10^{-10}$
XMM-Newton	0302970801	0.160	0.7 ± 0.3	20^{+4}_{-3}	$1.8^{+0.3}_{-0.2} \times 10^{-12}$
XMM-Newton	0302970601	0.426	$1.6^{+0.6}_{-0.5}$	22^{+6}_{-5}	$1.7^{+1.9}_{-0.6} \times 10^{-12}$
Chandra	10512	0.748	0.4 ± 0.2	9^{+10}_{-8}	$9.6^{+4.2}_{-3.8} \times 10^{-13}$
Chandra	2692	0.924	$-0.3^{+1.3}_{-0.9}$	13^{+11}_{-7}	$9.7^{+2.4}_{-2.1} \times 10^{-13}$
Swift	00609139000	0.991	2.0 ± 0.7	106^{+18}_{-17}	$1.9^{+5.8}_{-1.0} \times 10^{-9}$
Swift	00707545000	0.992	$-0.1^{+0.5}_{-0.7}$	31^{+10}_{-8}	$4.7^{+1.0}_{-0.7} \times 10^{-10}$
Swift	00745966000	0.996	0.4 ± 0.8	32^{+14}_{-11}	$6.0^{+3.9}_{-1.4} \times 10^{-10}$

Notes. [a]Unabsorbed X-ray fluxes in energy range 0.3−10 keV. [b]The fit parameters and flux obtained from a joint fit in range 0.3−10 keV.

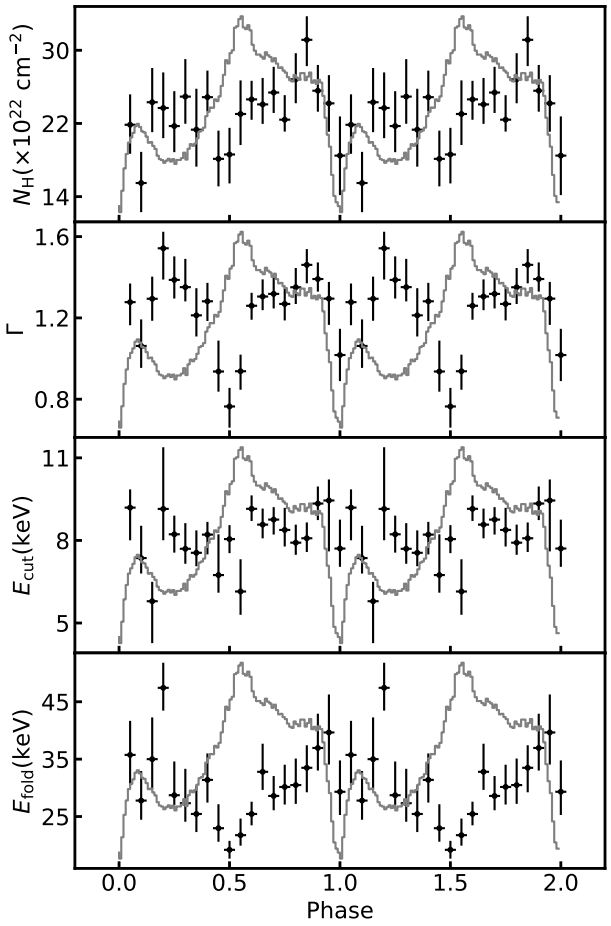

Fig. 5. Variations of the spectral parameters of the best-fit model as a function of pulse phase. The black crosses from the uppermost to the lowest panel show: neutral hydrogen column density N_H in units of 10^{22} cm^{-2}, photon index, cutoff energy, and folding energy. The full energy (3−79 keV) averaged pulse profile of the source is shown in gray in each panel. Errors are 1σ.

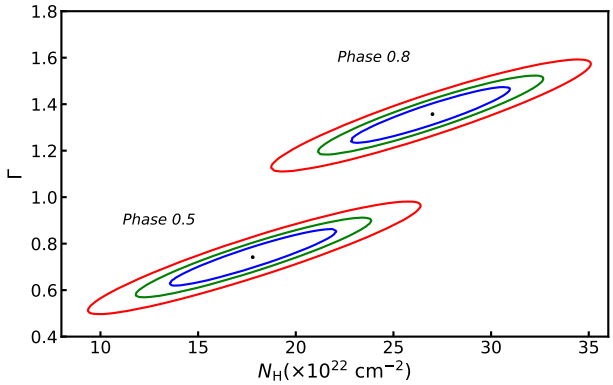

Fig. 6. Confidence contours of N_H versus Γ obtained using the best-fit model for the spin phase-resolved spectra at phases 0.5 and 0.8 (see the text). The blue, green, and red contours correspond to the 1σ, 2σ, and 3σ confidence levels obtained using χ^2 statistics for two free parameters.

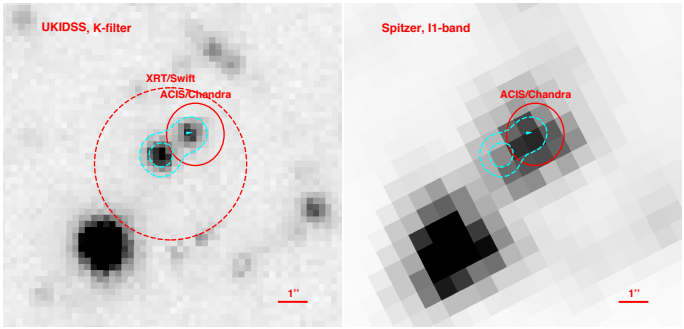

Fig. 7. Images of the sky around 2S 1845−024 in the *K*-filter obtained by the UKIRT telescope (GPS/UKIDSS sky survey, *left*) and in the 3.6μ-band obtained by the *Spitzer* telescope (*right*). The red circles indicate an uncertainty for the source position based on the *Swift* (dashed line) and *Chandra* (solid line) data, respectively. Cyan contours mark two IR objects closest to the X-ray position.

Unfortunately, having magnitudes only in two filters makes it challenging to draw any solid conclusions about the nature of the IR companion. However, the extinction A_K towards the system can be roughly estimated. According to Fig. 8, $A_K \simeq 4.1$ accounts for OB stars, including giants and supergiants, and $A_K \simeq 3.7$ for red giants. By converting these extinction magnitudes into the hydrogen column density N_H using the standard relations $A_V = 8.93 \times A_K$ (Cardelli et al. 1989) and $N_H = 2.87 \times 10^{21} \times A_V$ (Foight et al. 2016), we obtain

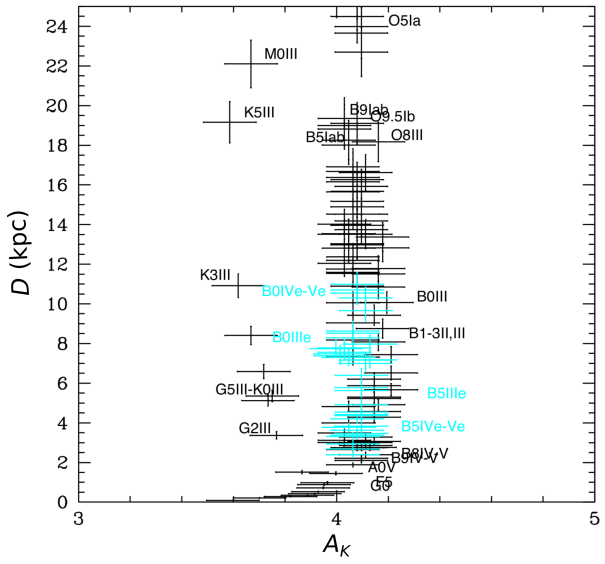

Fig. 8. Distance–extinction diagram showing how far away the star (black dots for normal and cyan for Be stars) of a specific class should be located if it is a counterpart of 2S 1845−024 and the appropriate extinction towards such a star.

$N_{\rm H} \simeq (10-11) \times 10^{22}\,{\rm cm}^{-2}$ for different types of the companion stars. At the same time, the X-ray spectrum revealed a significantly higher column density of $22.7 \times 10^{22}\,{\rm cm}^{-2}$, which is typical for highly absorbed HMXB systems (see, e.g., Rahoui et al. 2008). This circumstance may indicate that 2S 1845−024 belongs to this class of binary system.

To clarify the nature of the companion, we also used the mid-IR data obtained by the *Spitzer* telescope[14] (see Table 2). However, as can be seen from Fig. 7, there is another star located near the probable IR counterpart of 2S 1845−024. The spatial resolution of *Spitzer* did not allow us to fully resolve these objects (see cyan contours in Fig. 7), and therefore we were not able to exclude that the resulting mid-IR fluxes mentioned in Table 2 are affected by the confusion of these two stars.

Nevertheless, if we assume an OB supergiant (B9Iab, B5Iab, O5Ia etc.) to be the counterpart of 2S 1845−024, the distance to the source is expected to be more than ∼16 kpc (see Fig. 8). This is in line with the findings of Koyama et al. (1990a) who estimated a distance to the source of 10 kpc based on the high $N_{\rm H}$ value in the source spectrum. Our spectral analysis also supports these results as $N_{\rm H}$ shows variations on the orbital timescale from $\sim(1–2) \times 10^{23}\,{\rm cm}^{-2}$ at the phase around 0.5 to $\sim 10^{24}\,{\rm cm}^{-2}$ around the periastron passage. The lowest value of $N_{\rm H}$ is almost an order of magnitude higher than the Galactic mean value in the direction of the source. This fact along with a positive correlation of the $N_{\rm H}$ value with the X-ray flux points to the presence of a strong stellar wind in the system. Similar behavior is observed in other XRPs with hypergiant optical companions (e.g., for GX 301–2, Islam & Paul 2014). However, at the same time, we cannot rule out that the companion star is of another class. Thus, to reliably establish the nature of the IR companion of 2S 1845−024, spectroscopic observations in the near-IR band are required, for example with *K*-band spectroscopy. When the class of the companion star is established, we will be able to use the diagram shown in Fig. 8 to estimate the distance to the source with high accuracy.

[14] http://www.astro.wisc.edu/sirtf/

4. Discussion and conclusions

In this work, we present the results of the detailed X-ray and IR analysis of the poorly studied XRP 2S 1845−024 and its companion during the type I outburst of the source in 2017. For X-ray analysis, we used a single *NuSTAR* observation performed during the outburst and several X-ray observations obtained by *XMM-Newton*, *Chandra*, and *Swift*. For the IR analysis, data obtained from UKIDSS/GPS and *Spitzer*/GLIMPSE surveys were used.

In order to determine the magnetic field strength of the NS in the system, which was one of our primary goals, we searched for a possible cyclotron absorption line in the broad-band *NuSTAR* spectrum. Such a feature was not discovered in phase-averaged or in phase-resolved spectra of 2S 1845−024. Therefore, it can be inferred that either the line does not exist in the considered energy range or it is too weak to be detected with the current sensitivity of the observations. In the former case, considering the lower and upper limits of the operating energy-band of the *NuSTAR* instruments, we only can estimate the magnetic field strength of the source to be either weaker than $\sim 4 \times 10^{11}$ G or stronger than $\sim 7 \times 10^{12}$ G. Further sensitive observations are required to come to any solid conclusions.

In order to determine the nature of the companion and the distance to 2S 1845−024, we analyzed the IR data. However, the availability of the magnitudes only in two (*H* and *K*) filters limited us to roughly classifying the IR-companion in 2S 1845−024 as an OB-supergiant star located at a distance of more than ∼16 kpc. To establish a more accurate estimation of the nature of the IR companion in this system, as well as the distance to the source, sensitive spectroscopic observations in the near-IR band (e.g., *K*-band spectroscopy) are required. Our conclusion about the class of the optical companion is in agreement with the X-ray spectral properties of the source. The good coverage of the binary orbit with observations in the soft X-rays allowed us to investigate the variation of column density $N_{\rm H}$ as a function of orbital phase, which revealed the presence of a strong stellar wind in the system. However, we emphasize that an extensive study of the iron line is required to support this interpretation (see Islam & Paul 2014).

An estimation of the distance to 2S 1845−024 could also be obtained using the observed fluxes and presumable luminosity of the source in the different states. In particular, in the low state when the observed flux drops to about $10^{-12}\,{\rm erg\,s^{-1}\,cm^{-2}}$ (see Table 6), one can expect the luminosity of the source to be above $\sim 10^{34}\,{\rm erg\,s^{-1}}$ in the case of the ongoing accretion (Tsygankov et al. 2017, 2019) and, therefore, the distance to the system cannot be below ∼10 kpc. From another viewpoint, the peak luminosity during type-I outbursts from the transient XRPs can be of the order of $10^{37}\,{\rm erg\,s^{-1}}$. Taking into account the maximal observed flux from 2S 1845−024 of around $10^{-9}\,{\rm erg\,s^{-1}\,cm^{-2}}$ one can estimate the upper limit on the distance as ∼15 kpc. These rough estimates agree with results obtained from the IR data.

Acknowledgements. This work was supported by the grant 14.W03.31.0021 of the Ministry of Science and Higher Education of the Russian Federation. We also acknowledge the support from the Finnish Cultural Foundation through project number 00200764 and 85201677 (AN), the Academy of Finland travel grants 317552, 322779, 324550, 331951, and 333112, the National Natural Science Foundation of China grants 1217030159, 11733009, U2038101, U1938103, and the Guangdong Major Project of the Basic and Applied Basic Research grant 2019B030302001 (LJ). This work is based in part on data of the UKIRT Infrared Deep Sky Survey. Also, part of this work is based on observations made with the *Spitzer* Space Telescope, which is operated by the Jet Propulsion Laboratory, California Institute of Technology under a contract with NASA.

References

Boldin, P. A., Tsygankov, S. S., & Lutovinov, A. A. 2013, Astron. Lett., 39, 375
Burrows, D. N., Hill, J. E., Nousek, J. A., et al. 2005, Space Sci. Rev., 120, 165
Cardelli, J. A., Clayton, G. C., & Mathis, J. S. 1989, ApJ, 345, 245
Carpenter, J. M. 2001, AJ, 121, 2851
Corbet, R. H. D. 1986, MNRAS, 220, 1047
Doroshenko, V. A., Doroshenko, R. F., Postnov, K. A., Cherepashchuk, A. M., & Tsygankov, S. S. 2008, Astron. Rep., 52, 138
Doroshenko, V., Tsygankov, S., Long, J., et al. 2020, A&A, 634, A89
Evans, P. A., Beardmore, A. P., Page, K. L., et al. 2009, MNRAS, 397, 1177
Filippova, E. V., Tsygankov, S. S., Lutovinov, A. A., & Sunyaev, R. A. 2005, Astron. Lett., 31, 729
Finger, M. H., Bildsten, L., Chakrabarty, D., et al. 1999, ApJ, 517, 449
Foight, D. R., Güver, T., Özel, F., & Slane, P. O. 2016, ApJ, 826, 66
Gehrels, N., Chincarini, G., Giommi, P., et al. 2004, ApJ, 611, 1005
Harrison, F. A., Craig, W. W., Christensen, F. E., et al. 2013, ApJ, 770, 103
Islam, N., & Paul, B. 2014, MNRAS, 441, 2539
Jansen, F., Lumb, D., Altieri, B., et al. 2001, A&A, 365, L1
Karasev, D. I., Tsygankov, S. S., & Lutovinov, A. A. 2015, Astron. Lett., 41, 394
Koyama, K., Kunieda, H., Takeuchi, Y., & Tawara, Y. 1990a, PASJ, 42, L59
Koyama, K., Kawada, M., Kunieda, H., Tawara, Y., & Takeuchi, Y. 1990b, Nature, 343, 148
Lutovinov, A. A., & Tsygankov, S. S. 2009, Astron. Lett., 35, 433
Makino, F., & GINGA Team 1988, IAU Circ., 4661, 2
Malacaria, C., Jenke, P., Roberts, O. J., et al. 2020, ApJ, 896, 90
Nabizadeh, A., Tsygankov, S. S., Karasev, D. I., et al. 2019, A&A, 622, A198
Rahoui, F., Chaty, S., Lagage, P. O., & Pantin, E. 2008, A&A, 484, 801
Titarchuk, L. 1994, ApJ, 434, 570
Tsygankov, S. S., Mushtukov, A. A., Suleimanov, V. F., et al. 2017, A&A, 608, A17
Tsygankov, S. S., Doroshenko, V., Mushtukov, A. A., Lutovinov, A. A., & Poutanen, J. 2019, A&A, 621, A134
Verner, D. A., Ferland, G. J., Korista, K. T., & Yakovlev, D. G. 1996, ApJ, 465, 487
Wachter, K., Leach, R., & Kellogg, E. 1979, ApJ, 230, 274
Wegner, W. 2000, MNRAS, 319, 771
Wegner, W. 2006, MNRAS, 371, 185
Wegner, W. 2007, MNRAS, 374, 1549
Wegner, W. 2014, Acta Astron., 64, 261
Wegner, W. 2015, Astron. Nachr., 336, 159
Willingale, R., Starling, R. L. C., Beardmore, A. P., Tanvir, N. R., & O'Brien, P. T. 2013, MNRAS, 431, 394
Wilms, J., Allen, A., & McCray, R. 2000, ApJ, 542, 914
Zhang, S. N., Harmon, B. A., Paciesas, W. S., et al. 1996, A&AS, 120, 227